



OIST

OKINAWA INSTITUTE OF SCIENCE AND TECHNOLOGY GRADUATE UNIVERSITY  
沖縄科学技術大学院大学



# Structural Characterisation of Dimeric Esters in $\alpha$ -Pinene Secondary Organic Aerosol Using N<sub>2</sub> and CO<sub>2</sub> Ion Mobility Mass Spectrometry

Author	Yoshiteru Iinuma, Sathiyamurthi Ramasamy, Kei Sato, Agata Kolodziejczyk, Rafal Szmigielski
journal or publication title	Atmosphere
volume	12
number	1
page range	17
year	2020-12-24
Publisher	MDPI
Rights	(C) 2020 The Author(s).
Author's flag	publisher
URL	<a href="http://id.nii.ac.jp/1394/00001749/">http://id.nii.ac.jp/1394/00001749/</a>

doi: info:doi/10.3390/atmos12010017

## Article

# Structural Characterisation of Dimeric Esters in $\alpha$ -Pinene Secondary Organic Aerosol Using $N_2$ and $CO_2$ Ion Mobility Mass Spectrometry

 Yoshiteru Iinuma <sup>1,\*</sup> , Sathiyamurthi Ramasamy <sup>2,†</sup>, Kei Sato <sup>2</sup> , Agata Kołodziejczyk <sup>3,‡</sup> and Rafal Szmigielski <sup>3</sup>
<sup>1</sup> Okinawa Institute of Science and Technology Graduate University, Onna-son, Okinawa 904-0495, Japan

<sup>2</sup> National Institute for Environmental Studies, Tsukuba, Ibaraki 305-8506, Japan; sathiyamurthi@nies.go.jp or sathiyamurthi.ramasamy@ircelyon.univ-lyon1.fr (S.R.); kei@nies.go.jp (K.S.)

<sup>3</sup> Institute of Physical Chemistry of the Polish Academy of Sciences, 01-224 Warsaw, Poland; akolodziejczyk@ichf.edu.pl or agata@tropos.de (A.K.); ralf@ichf.edu.pl (R.S.)

\* Correspondence: yoshiteru.iinuma@oist.jp

† Currently Institut de recherches sur la catalyse et l'environnement de Lyon (IRCELYON), 69100 Villeurbanne, France.

‡ Currently at Leibniz-Institut für Troposphärenforschung, D-04318 Leipzig, Germany.

**Abstract:** The atmospheric oxidation of monoterpenes leads to the formation of secondary organic aerosol (SOA). While numerous works have been carried out in the past to characterise SOA at a molecular level, the structural elucidation of SOA compounds remains challenging owing to the lack of authentic standard compounds. In this work, the structures of  $\alpha$ -pinene originating dimeric esters in SOA with  $m/z$  357 ( $C_{17}H_{25}O_8^-$ ) and  $m/z$  367 ( $C_{19}H_{27}O_7^-$ ) were characterised using UPLC/ESI(-)IMS-TOFMS<sup>2</sup> (ultra-performance liquid chromatography coupled to ion mobility spectrometry tandem time-of-flight mass spectrometry). The measured collision cross-section ( $\Omega_{N_2}$ ) values were compared to theoretically calculated  $\Omega_{N_2}$  values. Selected product ions of dimeric compounds and the authentic standard compounds of product ions were subjected to  $CO_2$ -IMS-TOFMS for more detailed structural characterisation. Our results were consistent with previously reported subunits of the  $m/z$  357 (terpenylic acid and *cis*-pinic acid), and the  $m/z$  367 (10-hydroxy-*cis*-pinonic acid and *cis*-pinic acid) ions. The measured and calculated  $\Omega_{N_2}$  values of  $m/z$  367 ions further support the conclusion of earlier structural characterisation; however, the structure of the  $m/z$  357 ion remains vague and requires further characterisation studies with a synthesised reference compound.

**Keywords:** SOA; ion mobility; collision cross-section;  $\alpha$ -pinene SOA dimers; stereochemical assignment



**Citation:** Iinuma, Y.; Ramasamy, S.; Sato, K.; Kołodziejczyk, A.; Szmigielski, R. Structural Characterisation of Dimeric Esters in  $\alpha$ -Pinene Secondary Organic Aerosol Using  $N_2$  and  $CO_2$  Ion Mobility Mass Spectrometry. *Atmosphere* **2021**, *12*, 17. <https://dx.doi.org/10.3390/atmos12010017>

Received: 13 November 2020

Accepted: 20 December 2020

Published: 24 December 2020

**Publisher's Note:** MDPI stays neutral with regard to jurisdictional claims in published maps and institutional affiliations.



**Copyright:** © 2020 by the authors. Licensee MDPI, Basel, Switzerland. This article is an open access article distributed under the terms and conditions of the Creative Commons Attribution (CC BY) license (<https://creativecommons.org/licenses/by/4.0/>).

## 1. Introduction

Secondary organic aerosol (SOA) plays an important role in the Earth's climate system by directly or indirectly influencing the planetary energy budget [1]. Besides affecting air quality by reducing visibility, SOA can also potentially damage human health through the inhalation of ultrafine particles to the deepest part of the lungs [2,3]. Annual SOA production can be as high as 910 TgC yr<sup>-1</sup> [4], although this estimation is largely uncertain due to a lack of knowledge about the mechanisms leading to SOA formation [1].

Among various known SOA precursor compounds, monoterpenes have been studied extensively because they are emitted in large amounts with an estimated global emission of 155 Tg yr<sup>-1</sup> [5], and their oxidation products are found in fine ambient particles at considerable levels [6]. Ambient and laboratory monoterpene SOA compounds reported in the literature include multifunctional carboxylic acids, organosulfates, nitrooxy-organosulfates, highly oxidised organic molecules with peroxy functional groups (HOMs), and dimeric esters [6]. While some of these compounds are firmly identified by comparison to authentic standard compounds, many of them remain structurally uncharacterised due to difficulties

associated with the synthesis of standard compounds. This hinders our understanding of underlying processes leading to the formation of monoterpene SOA compounds in the atmosphere.

When no authentic standard compound is available for unambiguous identification of a target compound, tandem mass spectrometry ( $MS^n$ ) experiments are often performed to obtain a piece of structural information such as the presence of functional groups and structural subunits [7]. While  $MS^n$  is a powerful tool, it can lead to different structural matches for the same compound as the technique is highly dependent on instrumental settings and the interpretation of the mass spectra; it also does not provide information about three-dimensional conformation [8]. One of the ways to support structural identification is to obtain information about the conformation or shape of an ion using advanced mass spectrometric data. For this purpose, ion mobility spectrometry coupled to time-of-flight mass spectrometry (IMS-TOFMS) is often used to obtain information about the shape besides the elemental formula of a target ion. The IMS-HRMS measures ion mobility, i.e., drift velocity of an ion in an inert gas under the influence of an electric field. Ion mobility can be related to collisional cross-section ( $\Omega_{N_2}$ ), a physicochemical property related to the shape of an ion in the gas phase. This technique is increasingly used in the structural characterisation of small molecules since the introduction of the first commercial IMS-TOFMS in 2006 [9]. In the field of atmospheric science, IMS-TOFMS is successfully used for the molecular characterisation of  $\beta$ -pinene originating organosulfates [10], isoprene originating organosulfates [11], aerosol bound alkyl nitrates [12], classification of atmospherically relevant organic compounds [13], aqueous phase oligomerisation of  $\alpha,\beta$ -unsaturated carbonyls and acids [14], separation of highly oxygenated molecules in laboratory-generated  $\alpha$ -pinene SOA [15], particle-phase reaction products of  $\alpha$ -pinene oxidation [16], and heterogeneous oxidation of organic aerosols [17,18].

Past studies showed that dimeric esters with Mw 358 ( $C_{17}H_{26}O_8$ ) and Mw 368 ( $C_{19}H_{28}O_7$ ) are commonly found in laboratory-generated  $\alpha$ -pinene SOA [19–22]. They were also found in fine ambient particles influenced by boreal forest emissions [21,23–26], indicating that they contribute importantly to atmospheric SOA mass. The formation mechanisms of these dimeric esters remain uncertain to date, although several mechanisms are proposed in the literature. These include particle-phase esterification of carboxylic acids such as *cis*-pinic acid and terpenylic acid leading to Mw 358 [21], a gas phase mechanism involving Criegee intermediates [23], and the formation of  $RO_3R'$  from the reaction of  $RO_2\cdot$  and  $R'O\cdot$ , and the subsequent decomposition of acyl hydroperoxide groups to form stable esters [19]. Other suggested mechanisms that can lead to dimeric SOA compounds that are not exclusive to Mw 358 and Mw 368 include heterogeneous reactions of aldehydes with hydroperoxides [27,28], and more recently a series of organic peroxy and alkoxy radical cross-reactions at the interface forming dimeric compounds [17]. Recent mass spectrometric studies on  $\alpha$ -pinene SOA showed that these dimers consist of diaterpenylic acid and *cis*-pinic acid for Mw 358 [19–21] and of *cis*-hydroxyl pinonic acid and *cis*-pinic acid for Mw 368 [19]. While their monomeric units are unambiguously determined from  $MS^2$  data, further structural information is required for the determination of their exact conformations and configuration isomers. Such information is especially important for understanding the mechanisms leading to the formation of these compounds, and their roles in particle growth and SOA formation as the conformation of molecules are vital to the condensation process by their influence in inter- and intra-molecular interactions.

In this study, dimeric compounds with Mw 358 and Mw 368 present in laboratory-generated  $\alpha$ -pinene SOA were subjected to detailed structural re-elucidation experiments using IMS-TOFMS. Two types of drift gases were compared for the separation of ions in IMS-TOFMS: nitrogen ( $N_2$ ) and carbon dioxide ( $CO_2$ ). It is known that highly polarisable  $CO_2$  drift gas has different selectivity from  $N_2$  drift gas for smaller ions in IMS, e.g., [29–33]. By using  $CO_2$  drift gas, we expected to separate the small product ions of dimeric esters better in IMS-TOFMS<sup>2</sup>, enabling us to gather information about the conformation of these compounds.

## 2. Experiments

### 2.1. $\alpha$ -Pinene/O<sub>3</sub> SOA Sample Generation and SOA Standard Compound Synthesis

An  $\alpha$ -pinene ozonolysis experiment was conducted in a temperature controllable 6 m<sup>3</sup> Teflon<sup>®</sup> coated stainless steel chamber (ULVAC, Inc., Chigasaki, Japan) at National Institute of Environmental Studies (NIES), Tsukuba, Japan. Detailed explanation of the chamber setup can be found elsewhere [34–36]. SOA was produced from the reaction of 0.19 ppm of  $\alpha$ -pinene and 0.21 ppm of ozone. The SOA sample was collected on 47mm Teflon filter (total 0.21 mg, 1 m<sup>3</sup>) and stored below –22 °C until sample analysis.

A standard compound of terpenylic acid was synthesised following a method described in Claeys et al., 2009 [37]. The synthesis methods of *cis*-pinic acid and *cis*-norpinic acid can be found in Kołodziejczyk et al., 2019 [38].

### 2.2. Sample Analysis

A portion (2 × 1 cm diameter punch) of a collected filter was extracted in 1 mL of acetonitrile (QTofMS grade, Fujifilm Wako, Tokyo, Japan) using an orbital shaker. Insoluble debris was removed using a PTFE syringe filter (Millex LG 0.20 µm, Merck, Darmstadt, Germany). The extract was dried using a vacuum concentrator and reconstituted in 200 µL of 1:1 acetonitrile/ultrapure water (*v/v*) solution.

Ultra-performance liquid chromatography (UPLC, Acquity I-Class, Waters, MA, USA) equipped with a Waters Acquity UPLC T3 column (2.1 mm × 100 mm, 100Å, 1.8 µm) was used to separate dimeric esters. The eluent programme used was as follows: 99% (A) ultrapure water with 0.1% formic acid and 1% (B) acetonitrile for 2 min, raised (B) to 100% (B) in 5.5 min, kept constant for 2.5 min, brought back to the initial condition and equilibrated for 3.5 min. The flow rate of the eluent was 0.4 mLmin<sup>−1</sup>, and the injection volume of the sample was 1 µL. The column temperature was kept at 30 °C, and the sample compartment was kept at 15 °C.

The ion mobilities of dimeric esters were measured using electrospray ionisation ion mobility spectrometry time-of-flight mass spectrometry in the negative ion mode (ESI(-)-IMS-QTOFMS, Synapt G2S, Waters). All ions reported in this study are (M-H)<sup>−</sup> ions. The operational principle of Synapt G2S ESI-IMS-QTOFMS is as follows: The ions formed in the electrospray ionisation source entered through the entrance orifice to the ion guide, then to the quadrupole mass filter. The filtered or non-filtered ions are passed to the “TriWave” region that consists of a trap ion guide, an ion mobility spectrometer (IMS), and a transfer ion guide. Collision induced dissociation (CID) experiments can be performed in both the trap and transfer ion guides though only the trap was used for CID experiments in this study. This means that a precursor ion and product ions were detected at different drift times, enabling us to obtain collision cross-section ( $\Omega$ ) values of precursor and product ions simultaneously. After the transfer ion guide, the ions were passed into the Time-of-Flight (TOF) analyser and the detector to record *m/z* values of the ions. The IMS-QTOFMS parameters used for the ion mobility separation are summarised in Table 1.

The purities of the buffer gases used were 99.9995% for N<sub>2</sub> made from an N<sub>2</sub> generator (KURASEP, Kuraray Chemical, Japan) and 95.5% for CO<sub>2</sub> (Iwatani, Japan). The Waters Synapt G2S system was not equipped with a thermostated jacket to keep the drift tube temperature constant. However, our laboratory was kept at 25 °C to minimise temperature related drift time fluctuation.

To adjust the day-to-day variation of drift times for N<sub>2</sub>-IMS and CO<sub>2</sub>-IMS, a Waters Major Mix IMS/ToF Calibration Kit (Waters, MA, USA) containing standard compounds with known nitrogen collision cross-section ( $\Omega_{N_2}$ ) values was used. These were acetaminophen (C<sub>8</sub>H<sub>8</sub>NO<sub>2</sub><sup>−</sup>, *m/z* 150.0555,  $\Omega_{N_2}$  = 131.5), sulfaguanidine (C<sub>7</sub>H<sub>9</sub>N<sub>4</sub>O<sub>2</sub>S<sup>−</sup>, *m/z* 213.0446,  $\Omega_{N_2}$  = 145.2), sulfadimethoxine (C<sub>12</sub>H<sub>13</sub>N<sub>4</sub>O<sub>4</sub>S<sup>−</sup>, *m/z* 309.0658,  $\Omega_{N_2}$  = 170.1), and Val-Tyr-Val (C<sub>19</sub>H<sub>28</sub>N<sub>3</sub>O<sub>5</sub><sup>−</sup>, *m/z* 378.2029,  $\Omega_{N_2}$  = 192.5). In all experimental days, the drift times of standard compounds stayed the same when the operational conditions were the same (i.e., no deviation of drift time during the course of the analytical day). It is noted that  $\Omega_{N_2}$  measurements using Synapt G2 instruments are highly reproducible, and less than 2%

relative standard deviation (RSD) for  $\Omega_{N_2}$  values of more than 100 common metabolites is reported from an inter-laboratory comparison study [39].

**Table 1.** Operating conditions for ESI(-)-IMS-QTOFMS.

Parameter	
Mass range ( $m/z$ )	50–1200
Capillary voltage (kV)	2.5
Sampling cone voltage (V)	40
Source offset (V)	10
Source temperature ( $^{\circ}\text{C}$ )	120
Desolvation temperature ( $^{\circ}\text{C}$ )	350
Desolvation Gas Flow ( $\text{Lh}^{-1}$ )	800
Nebuliser Gas Flow (Bar)	6.5
Cone gas flow ( $\text{Lh}^{-1}$ )	50
IMS Cell Pressure (mbar)	3 ( $\text{N}_2$ ) 1.5 ( $\text{CO}_2$ )
Buffer gas flow rate ( $\text{mLmin}^{-1}$ )	90
IMS Wave height (V)	40
IMS Wave Velocity ( $\text{ms}^{-1}$ )	650
IMS resolution ( $\Omega/\Delta\Omega$ )	40
Trap Collision Energy (eV)	4
Transfer Collision Energy (eV)	2
Trap Collision Energy Ramp Start for $\text{MS}^2$ (eV)	15.0
Trap Collision Energy Ramp End for $\text{MS}^2$ (eV)	40.0

ESI(-)-IMS-QTOFMS: electrospray ionisation ion mobility spectrometry time-of-flight mass spectrometry in the negative ion mode.

The calibration curve for the determination of  $\Omega_{N_2}$  values was constructed from the measurement of the same calibration standard solution. To obtain  $\Omega_{N_2}$  values of target analytes, we followed the procedure for  $\Omega_{N_2}$  calibration curve construction published in Paglia et al., 2014 [39] and Paglia and Astarita, 2017 [40].

### 2.3. Theoretical Calculation of Collision Cross-Section

$\Omega_{N_2}$  values for Mw 358 and Mw 368 dimeric esters, and their  $\text{MS}^2$  product ions were calculated using  $\text{N}_2$ -MOBCAL reported by Campuzano et al. [41].  $\text{N}_2$ -MOBCAL is based on the MOBCAL developed by Mesleh et al. [42] for the calculation of  $\Omega_{\text{He}}$  based on a He trajectory method. To prepare an input file for the  $\text{N}_2$ -MOBCAL, we followed a method described in Campuzano et al. [41] except for the initial 2D structural drawing made via ChemDraw Professional ver. 16.0 (PerkinElmer, MA, USA). Owing to the lack of carbon dioxide collision cross-section values ( $\Omega_{\text{CO}_2}$ ) for reference compounds, no  $\Omega_{\text{CO}_2}$  values were calculated in this study.

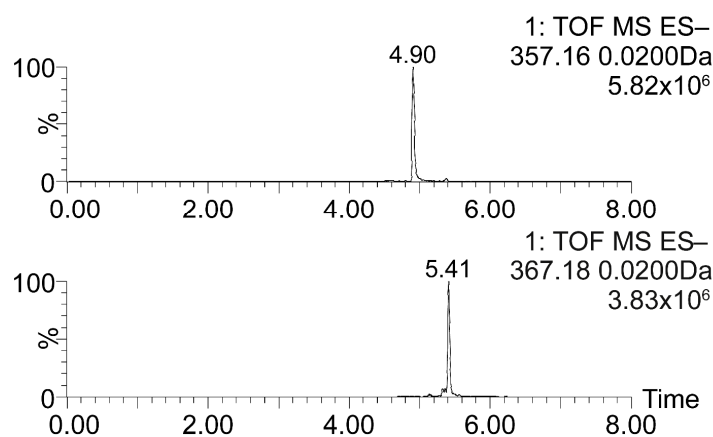
The accuracy of the  $\text{N}_2$ -MOBCAL for the class of compounds concerned in this study was assessed from the literature data. Paglia et al., 2014 [39] compared 107  $\Omega_{N_2}$  values of negatively charged ions predicted by  $\text{N}_2$ -MOBCAL to the measured  $\Omega_{N_2}$  values determined by three independent Synapt G2 instruments from different laboratories. Among their dataset, we selected 13 carboxylic acids (glyceric acid, fumaric acid, succinic acid, ketoleucine, malic acid, salicylic acid, oxoglutaric acid, mevalonic acid, aconitic acid, ascorbic acid, citric acid, glucuronic acid, and gluconic acid) and eight saccharides (fructose, galactose, glucose, mannose, mannitol, lactose, sucrose, and trehalose) that have the same functional groups (-OH or -COOH), elements (CHO), and similar  $m/z$  values as the compounds studied here for the assessment. In general, the  $\text{N}_2$ -MOBCAL predicted  $\Omega_{N_2}$  values agreed well with the measured  $\Omega_{N_2}$  values from all three Synapt G2 instruments, with average relative difference ( $\text{RD}\% = (\text{measured } \Omega - \text{predicted } \Omega)/(\text{measured } \Omega)$ ) values ranging from  $-0.1 \pm 4.0\%$  to  $-1.3 \pm 4.3\%$  ( $\mu \pm 1\sigma$ ). Worse  $\text{RD}\%$  values among all data were found from glyceric acid, fructose, and glucose with  $\text{RD}\%$  of 8.5–9.2, 6.8–10.8, and 6.0–10.1, respectively. These highly oxygenated compounds (a C/O ratio  $\geq 1$ ) may need further

molecular dynamic simulation to accurately represent their molecular conformations, and caution is warranted for the application of N<sub>2</sub>-MOBCAL for this class of compounds. Based on this, we concluded that N<sub>2</sub>-MOBCAL was suitable for the purpose of this study. In addition to a published dataset, we measured  $\Omega_{N_2}$  values of *cis*-norpinic acid, terpenylic acid, and *cis*-pinic acid, then compared them with N<sub>2</sub>-MOBCAL predicted  $\Omega_{N_2}$  values. The RD% values were 2.4% for terpenylic acid (IMS: 137.7 Å<sup>2</sup>, N<sub>2</sub>-MOBCAL: 134.4 Å<sup>2</sup>), 1.0% for *cis*-norpinic acid (IMS: 136.6 Å<sup>2</sup>, N<sub>2</sub>-MOBCAL: 135.3 Å<sup>2</sup>), and 4.5% for *cis*-pinic acid (IMS: 140.6 Å<sup>2</sup>, N<sub>2</sub>-MOBCAL: 147.0 Å<sup>2</sup>). These RD% values fall within the range of RD% values obtained from the dataset of Paglia et al., 2014 [39], except for *cis*-pinic acid. This discrepancy is discussed in a later section.

### 3. Results and Discussion

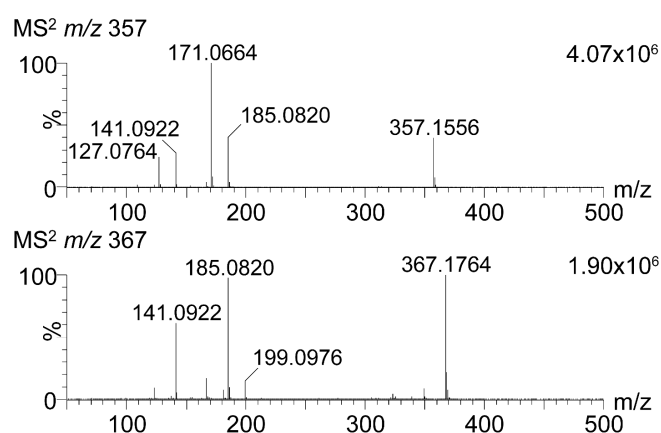
#### 3.1. Tandem Mass Spectrometry Analysis of *m/z* 357 (C<sub>17</sub>H<sub>25</sub>O<sub>8</sub><sup>-</sup>) and *m/z* 367 (C<sub>19</sub>H<sub>27</sub>O<sub>7</sub><sup>-</sup>) Ions

Figure 1 shows the extracted ion chromatograms (EICs) of *m/z* 357 (C<sub>17</sub>H<sub>25</sub>O<sub>8</sub><sup>-</sup>) and *m/z* 367 (C<sub>19</sub>H<sub>27</sub>O<sub>7</sub><sup>-</sup>) ions detected in a chamber-generated  $\alpha$ -pinene/O<sub>3</sub> SOA sample. The EICs showed that no isobaric isomers of these dimers were present in the sample. Figure 2 shows the high-resolution tandem mass spectrometry data (MS<sup>2</sup>) of *m/z* 357 and *m/z* 367 ions detected at 4.90 min and 5.41 min, respectively. The MS<sup>2</sup> product ions of *m/z* 357 were *m/z* 185 (C<sub>9</sub>H<sub>13</sub>O<sub>4</sub><sup>-</sup>), *m/z* 171 (C<sub>8</sub>H<sub>11</sub>O<sub>4</sub><sup>-</sup>), *m/z* 141 (C<sub>8</sub>H<sub>13</sub>O<sub>2</sub><sup>-</sup>), and *m/z* 127 (C<sub>7</sub>H<sub>11</sub>O<sub>2</sub><sup>-</sup>). In the MS<sup>2</sup> data of *m/z* 367, product ions detected at a significant level were *m/z* 199 (C<sub>10</sub>H<sub>15</sub>O<sub>4</sub><sup>-</sup>), *m/z* 185 (C<sub>9</sub>H<sub>13</sub>O<sub>4</sub><sup>-</sup>), *m/z* 167 (C<sub>9</sub>H<sub>11</sub>O<sub>3</sub><sup>-</sup>), *m/z* 141 (C<sub>8</sub>H<sub>13</sub>O<sub>2</sub><sup>-</sup>), and *m/z* 123 (C<sub>8</sub>H<sub>11</sub>O<sup>-</sup>). These product ions were consistent with published data in the literature [19,21,43], although their relative intensities were not the same as the literature data owing to the difference in an MS<sup>2</sup> experiment condition in each study. While the product ions were the same, MS<sup>2</sup> data alone does not provide sufficient evidence to unambiguously confirm the structures of the two dimers. To obtain further structural information, these ions were subjected to IMS-TOFMS analysis.



**Figure 1.** Extracted ion chromatograms (EICs) of *m/z* 357 (C<sub>17</sub>H<sub>25</sub>O<sub>8</sub><sup>-</sup>, top panel) and *m/z* 367 (C<sub>19</sub>H<sub>27</sub>O<sub>7</sub><sup>-</sup>, bottom panel) ions detected in laboratory-generated  $\alpha$ -pinene/O<sub>3</sub> sample. The time axis is in minutes.





**Figure 2.** High-resolution tandem mass spectrometric data of  $m/z$  357 ( $C_{17}H_{25}O_8^-$ , top panel) and  $m/z$  367 ( $C_{19}H_{27}O_7^-$ , bottom panel) ions detected in laboratory-generated  $\alpha$ -pinene/ $O_3$  sample.

### 3.2. Ion Mobility Spectrometry Tandem Mass Spectrometry Analysis of $m/z$ 357 ( $C_{17}H_{25}O_8^-$ ) and $m/z$ 367 ( $C_{19}H_{27}O_7^-$ ) Ions

#### 3.2.1. $N_2$ -IMS-TOFMS<sup>2</sup> of $m/z$ 357 ( $C_{17}H_{25}O_8^-$ ) Ion

The  $N_2$  driftgrams of the major product ions detected in the MS<sup>2</sup> experiment of  $m/z$  357 ion are shown in Figure 3. Both Müller et al., 2009 [43] and Kahnt et al., 2018 [19] attributed the  $m/z$  185 product ion to *cis*-pinic acid though they assigned the  $m/z$  171 product ion to a different product ion; Müller et al., 2009 [43] assigned it to *cis*-norpinic acid, whereas Kahnt et al., 2018 [19] assigned it to a diaterpenylic acid. To assign the structures of product ions unambiguously,  $N_2$  drift times of *cis*-pinic acid, *cis*-norpinic acid, and terpenylic acid was compared to those of product ions (Figure 4). The  $m/z$  185 product ion showed the identical drift time as the standard of *cis*-pinic acid (1.41), indicating that the product ion was indeed *cis*-pinic acid. The drift time of the  $m/z$  171 product ion also agreed well with those of  $m/z$  171 producing standard compounds; however, the product ion, *cis*-norpinic acid, and terpenylic acid produced the same drift time (1.30 msec) and could not be assigned to the definitive structure based on the results from  $N_2$ -IMS-QTOFMS<sup>2</sup> experiments. To better distinguish *cis*-norpinic acid and terpenylic acid, the  $m/z$  357 ion and their MS<sup>2</sup> product ions were analysed using  $CO_2$  as a buffer gas for the ion mobility separation ( $CO_2$ -IMS-QTOFMS<sup>2</sup>).

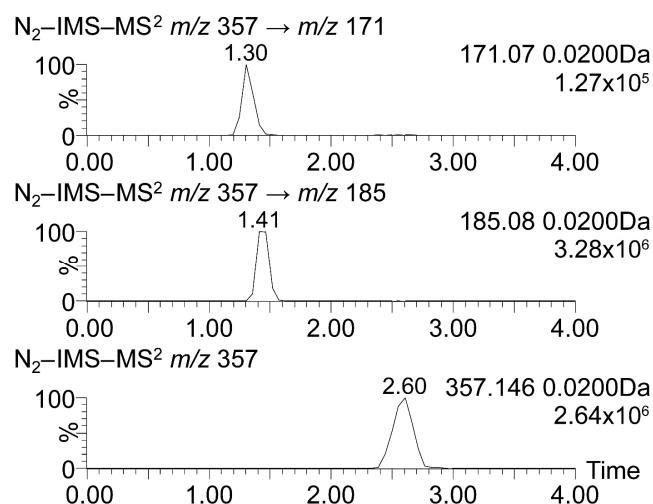


**Figure 3.**  $N_2$ -driftgrams of precursor and major product ions originating from  $m/z$  357 ion. The top panel shows  $m/z$  171 ( $C_8H_{11}O_4^-$ ), the middle panel shows  $m/z$  185 ( $C_9H_{13}O_4^-$ ), and the bottom panel shows  $m/z$  357 ( $C_{17}H_{25}O_8^-$ ). The time axis is in milliseconds.

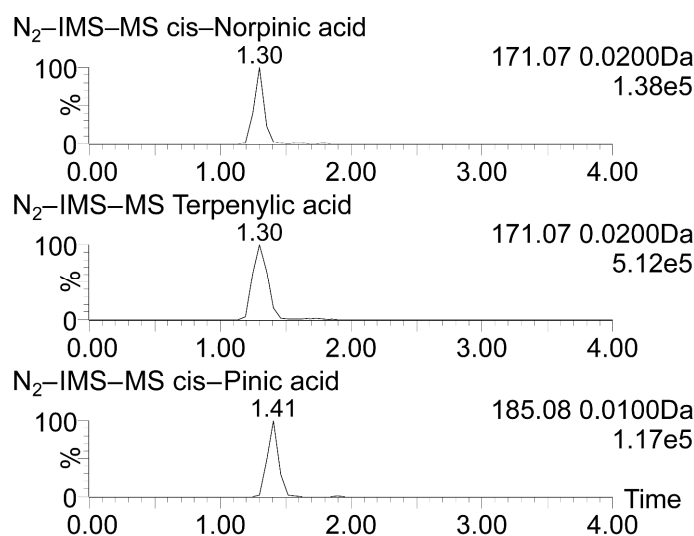


**Figure 4.**  $N_2$ -driftgrams of standard compounds. The top panel shows *cis*-norpinic acid ( $m/z$  171,  $C_8H_{11}O_4^-$ ), the middle panel shows terpenylic acid ( $m/z$  171,  $C_8H_{11}O_4^-$ ), and the bottom panel shows *cis*-pinic acid ( $m/z$  185,  $C_9H_{13}O_4^-$ ). The time axis is in milliseconds.

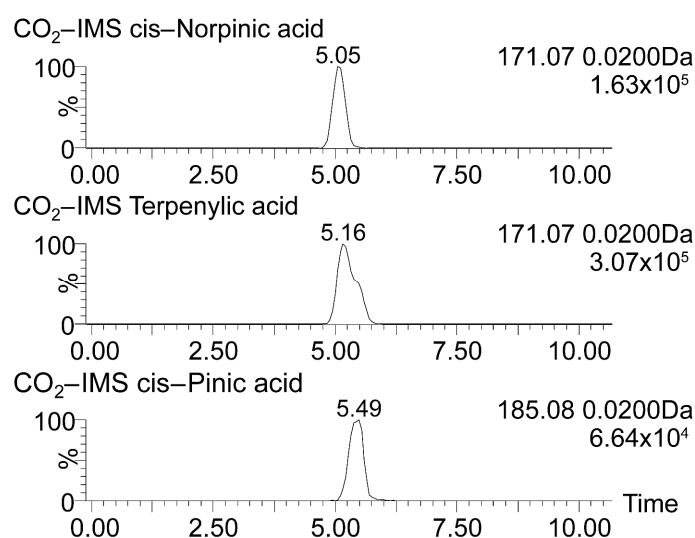
### 3.2.2. $CO_2$ -IMS-TOFMS<sup>2</sup> of $m/z$ 357 ( $C_{17}H_{25}O_8^-$ ) Ion

Figure 5 shows the  $CO_2$  driftgrams of (a) *cis*-norpinic acid, (b) terpenylic acid, and (c) *cis*-pinic acid. As can be seen, the utilisation of a larger and more polarisable  $CO_2$  drift gas separated *cis*-norpinic acid and terpenylic acid well enough, and their drift times can be used for the structural assignment of the  $m/z$  171 product ion. Figure 6 shows the driftgrams of the major product ions detected in the MS<sup>2</sup> experiment of  $m/z$  357 ion. Similar to the  $N_2$ -IMS-TOFMS<sup>2</sup> experiment, the  $CO_2$  drift time of *cis*-pinic acid was in line with that of the  $m/z$  185 product ion. For the  $m/z$  171 product ion, the  $CO_2$  drift time of terpenylic acid matched well with that of the  $m/z$  171 product ion. Note that  $CO_2$  drift times were highly reproducible and consistently detected as the same with no deviation. In addition to the main peak, the terpenylic acid and  $m/z$  171 product ion showed a shoulder peak that appeared to encounter another ion. However, the driftgram shown in Figures 5 and 6 were selected ion driftgrams with an  $m/z$  0.02 window; hence it was unlikely that these peaks were contaminated by other ions. One possible explanation for the shoulder peak is that it originated from an open ring structure of terpenylic acid that may have formed in the TriWave region of the instrument. It is known that a travelling wave ion mobility instrument such as Synapt suffers from ion activation due to ion heating, and this causes conformational changes and/or dissociation of the ions to some extent. Further investigation is necessary for the exact cause of the shoulder peak for terpenylic acid and the  $m/z$  171 product ion.

It has been reported that the structure producing the  $m/z$  171 ion from the  $m/z$  357 ion is diaterpenylic acid, which has the non-lactone structure of terpenylic acid [19]. Based on the drift times of the  $m/z$  171 product ion and terpenylic acid, it is likely that the  $m/z$  171 product ion (diaterpenylic acid) led to cyclisation, forming terpenylic acid after collision-induced dissociation during IMS-TOFMS<sup>2</sup> experimentation.

While  $N_2$ -IMS-TOFMS<sup>2</sup> and  $CO_2$ -IMS-TOFMS<sup>2</sup> experiments provided information about the structures of monomers, they do not provide information about the stereochemical representation of the molecular structure, such as *cis-trans* isomers or positional isomers. To assign the stereochemical structure of the  $m/z$  357 ion, measured and theoretical  $\Omega_{N_2}$  values for previously reported structures were compared, and the results are discussed in Section 3.3.





**Figure 5.** CO<sub>2</sub>- driftgrams of standard compounds. The top panel shows *cis*-norpinic acid ( $m/z$  171, C<sub>8</sub>H<sub>11</sub>O<sub>4</sub><sup>-</sup>), the middle panel shows terpenylic acid ( $m/z$  171, C<sub>8</sub>H<sub>11</sub>O<sub>4</sub><sup>-</sup>), and the bottom panel shows *cis*-pinic acid ( $m/z$  185, C<sub>9</sub>H<sub>13</sub>O<sub>4</sub><sup>-</sup>). The time axis is in milliseconds.

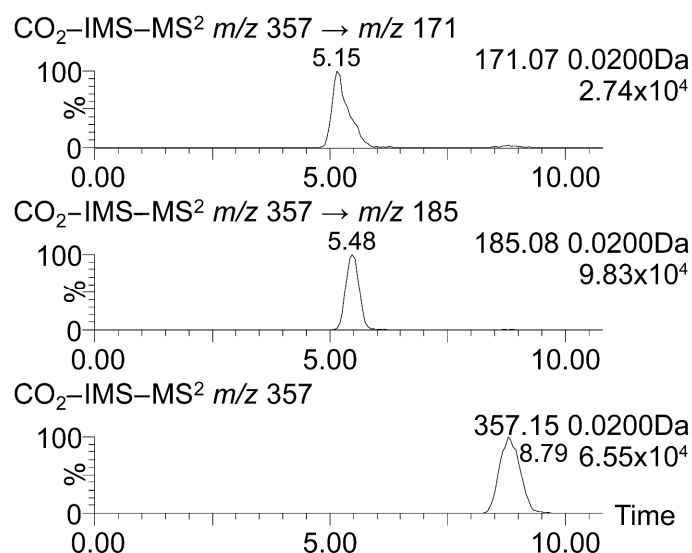


**Figure 6.** CO<sub>2</sub>- driftgrams of precursor and major product ions originating from the  $m/z$  357 ion. The top panel shows  $m/z$  171 (C<sub>8</sub>H<sub>11</sub>O<sub>4</sub><sup>-</sup>), the middle panel shows  $m/z$  185 (C<sub>9</sub>H<sub>13</sub>O<sub>4</sub><sup>-</sup>), and the bottom panel shows  $m/z$  357 (C<sub>17</sub>H<sub>25</sub>O<sub>8</sub><sup>-</sup>). The time axis is in milliseconds.

### 3.2.3. N<sub>2</sub>-IMS-TOFMS<sup>2</sup> of the $m/z$ 367 (C<sub>19</sub>H<sub>27</sub>O<sub>7</sub><sup>-</sup>) Ion and the Structural Elucidation of the $m/z$ 199 Product Ion from Theoretical and Measured $\Omega_{N_2}$ Values

The driftgrams of product ions obtained from N<sub>2</sub>-IMS-TOFMS<sup>2</sup> experimentation for the  $m/z$  367 ion are shown in Figure 7. The drift time of the  $m/z$  185 product ion was identical to that of *cis*-pinic acid in Figure 3, confirming the presence of *cis*-pinic acid in the  $m/z$  367 ion. According to the literature data [19,44], the other product ion detected at  $m/z$  199 was likely 10-hydroxy-*cis*-pinonic acid; though no authentic standard compound was available for the positive identification of the  $m/z$  199 product ion for this study. To obtain further insights into the structure of the  $m/z$  199 product ion, a comparison was made between the theoretically calculated  $\Omega_{N_2}$  value of 10-hydroxy-*cis*-pinonic acid and the measured  $\Omega_{N_2}$  value of the  $m/z$  199 product ion.

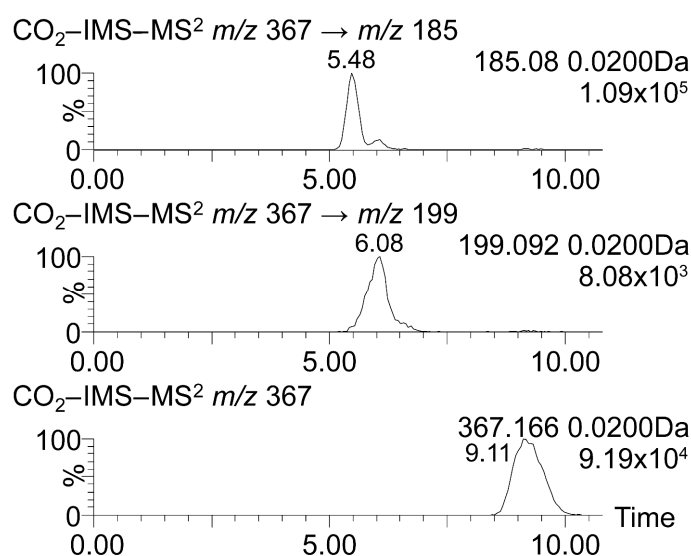


**Figure 7.**  $N_2$ -driftgrams of precursor and major product ions originating from the  $m/z$  367 ion. The top panel shows  $m/z$  185 ( $C_9H_{13}O_4^-$ ), the middle panel shows  $m/z$  199 ( $C_{10}H_{15}O_4^-$ ), and the bottom panel shows  $m/z$  367 ( $C_{19}H_{27}O_7^-$ ). The time axis is in milliseconds.

Table 2 summarises the theoretically calculated  $\Omega_{N_2}$  values of *cis*-pinic acid and 10-hydroxy-*cis*-pinonic acid, and measured  $\Omega_{N_2}$  values of  $m/z$  185 and  $m/z$  199 product ions from  $N_2$ -IMS-TOFMS<sup>2</sup> experiment for the  $m/z$  367 ion.

**Table 2.** Theoretical and measured  $\Omega_{N_2}$  values of product ions of  $m/z$  367 ( $C_{19}H_{27}O_7^-$ ) ion.

Name	Formula	$m/z$	$\Omega_{N_2}$ IMS ( $\text{\AA}^2$ )	$\Omega_{N_2}$ MOBCAL ( $\text{\AA}^2$ )	RD%
<i>cis</i> -pinic acid	$C_9H_{13}O_4^-$	185.0789	140.6	147.0	−4.5%
<i>cis</i> -pinic acid with an intramolecular hydrogen bond	"	"	"	141.7	−0.8%
10-Hydroxy- <i>cis</i> -pinonic acid	$C_{10}H_{15}O_4^-$	199.0931	144.3	142.2	1.48%

RD%: relative difference IMS: ion mobility spectrometry;  $\Omega_{N_2}$ : collision cross-section.

For the  $C_{10}H_{15}O_4^-$  product ion, the difference between the theoretical and measured  $\Omega_{N_2}$  values was within 1.5% relative difference. This agreement further supports the proposed structures of 10-hydroxy-*cis*-pinonic acid for the  $m/z$  199 compound. However, the unambiguous structural identification of the  $m/z$  199 product ion still requires comparison of the  $\Omega_{N_2}$  and  $\Omega_{CO_2}$  values between the standard compound of 10-hydroxy-*cis*-pinonic acid and the  $m/z$  199 product ion, as  $\Omega_{N_2}$  values may not be sufficiently different for all possible hydroxy-*cis*-pinonic acid isomers with the -OH group attached to a different position of the carbon skeleton.

Regarding the difference between the predicted and measured  $\Omega_{N_2}$  values of *cis*-pinic acid, RD% value was greater than those of terpenylic acid, *cis*-norpinic acid, and 10-hydroxy-*cis*-pinic acid. As described in Section 2.3 about the prediction of  $\Omega_{N_2}$  values, RD% values of the measured and the predicted  $\Omega_{N_2}$  values could be larger than 10% for some of the highly oxygenated compounds, though the C/O ratio of *cis*-pinic acid was much lower than 1, and it is unlikely that the predicted  $\Omega_{N_2}$  value of *cis*-pinic acid was biased for this reason. The predicted  $\Omega_{N_2}$  value of *cis*-pinic acid became much closer to that of the measured value when an intra-molecular hydrogen bond between the carboxylate and carboxylic groups was considered in the modelled structural conformation, indicating the difficulties of associating with the geometrical optimisation for the prediction of  $\Omega_{N_2}$  values.

### 3.3. The Structural and the Conformation Elucidation of $m/z$ 357 and $m/z$ 367 Ions from Theoretical and Measured Values

The theoretical and measured  $\Omega_{N_2}$  values from  $N_2$ -IMS-TOFMS of  $m/z$  357 and 367 ions and their structures considered in this study are summarised in Table 3. In addition to the positional isomers (labelled as 357a, 357b, 367a, and 367b following Kahnt et al., 2018 [19]), we considered (*R,R*) and (*S,S*) stereoisomers of  $m/z$  357 ions, and (*S,S*)(*S,S*) and (*S,S*)(*R,R*) stereoisomers of  $m/z$  367 ions. We note that the  $m/z$  367 ion may have alternative structures that consist of *cis*-pinic acid and positional isomers of hydroxy-*cis*-pinonic acid. They were not considered in this study owing to the high computational expenses of  $\Omega_{N_2}$  prediction. For all modelled structures, theoretical  $\Omega_{N_2}$  values were much greater than those of measured  $m/z$  357 and  $m/z$  367 ions. As the drift times of product ions from  $N_2$ -IMS-TOFMS<sup>2</sup> and  $CO_2$ -IMS-TOFMS<sup>2</sup> experiments agreed very well with authentic standard compounds, it is likely that the discrepancy originates from the conformational isomerism of the  $m/z$  357 and  $m/z$  367 ions. Smaller measured  $\Omega_{N_2}$  values than the theoretically calculated values suggest that the  $m/z$  357 and  $m/z$  367 ions in the IMS instrument are more spherical in shape than the structures shown in Table 3. To determine the conformation of the  $m/z$  357 and  $m/z$  367 ions, additional conformational candidates were subjected to theoretical  $\Omega_{N_2}$  calculation. For this purpose, both the dimeric compounds were folded to make a clam shell structure by forming intra-molecular hydrogen bonding between terminal carboxyl groups (Table 4). As expected, the calculated  $\Omega_{N_2}$  values for the structures with a hydrogen bond became much closer to those of the measured  $\Omega_{N_2}$  values. Among all the structural candidates, 367bHB(*R,R*)(*S,S*) yielded sufficiently small RD of 1.42% to support the structures of the  $m/z$  367 ion. Among all the  $m/z$  357 structures, 357bHB(*S*)(*R,R*) resulted in the smallest RD of 2.35%. This supports the structural suggestion by Gao et al. (2010) [22] and Beck and Hoffmann (2016) [20] but contradicts the results of Yasmeen et al. (2010) [21] and Kahnt et al. (2018) [19] in which 357a is suggested as its structure based on the results obtained from LC/MS<sup>2</sup> experiments of a methylated  $m/z$  357 ion. While the theoretical  $\Omega_{N_2}$  value of the  $m/z$  357 ion supports the structure of 357b, the RD value over 2% is larger than the acceptance criterion of the calibration of the  $\Omega_{N_2}$  values for the instrument [45] and it remains too unclear for conclusive structural elucidation. Further stereochemical assignment study using the authentic standard compound is warranted to unambiguously elucidate the structure of the  $m/z$  357 ion.

**Table 3.** Structures and  $\Omega_{N_2}$  values of  $m/z$  357 and  $m/z$  367 ions considered in this study. The ditto mark (") indicates the formula or number is the same as above.

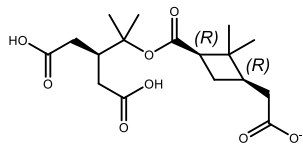
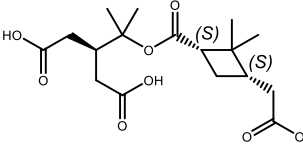
Abbreviation	Structure	$m/z$	$\Omega_{N_2}$ IMS ( $\text{\AA}^2$ )	$\Omega_{N_2}$ MOBCAL ( $\text{\AA}^2$ )	RD%	
357a( <i>R,R</i> )		$C_{17}H_{25}O_8^-$	357.1549	178.6	191.4	6.91%
357a( <i>S,S</i> )		"	"	"	209.8	16.07%

Table 3. Cont.

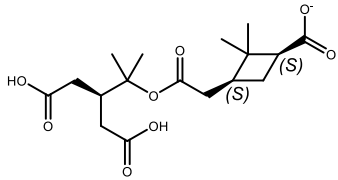
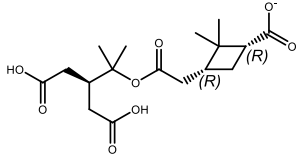
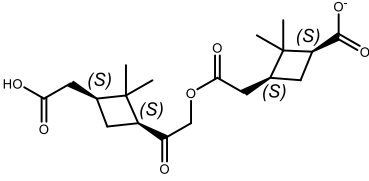
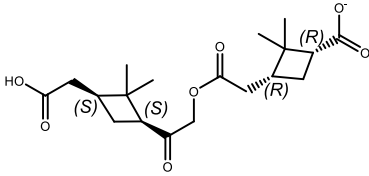
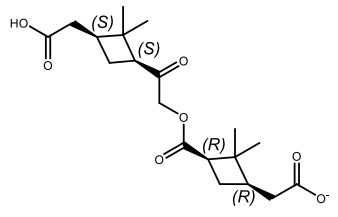
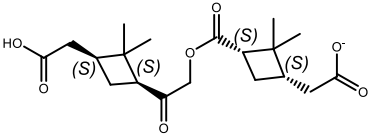
Abbreviation	Structure	$m/z$	$\Omega_{N_2}$ IMS ( $\text{\AA}^2$ )	$\Omega_{N_2}$ MOBCAL ( $\text{\AA}^2$ )	RD%	
357b(S,S)		"	"	"	195.1	8.83%
357b(R,R)		"	"	"	196.1	9.36%
367a(S,S)(S,S)		C <sub>19</sub> H <sub>27</sub> O <sub>7</sub> <sup>-</sup>	367.1757	182.5	216.4	16.99%
367a(S,S)(R,R)		"	"	"	227.5	21.93%
367b(S,S)(R,R)		"	"	"	205.7	11.95%
367b(S,S)(S,S)		"	"	"	201.1	9.69%

Table 4. Structures and  $\Omega_{N_2}$  values of  $m/z$  357 and  $m/z$  367 ions with an intra-molecular hydrogen bond considered in this study.

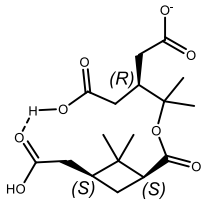
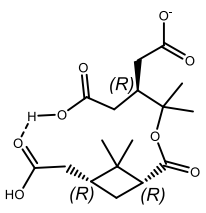
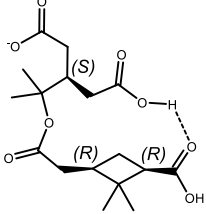
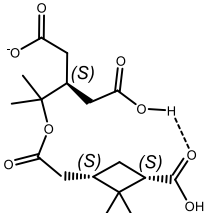
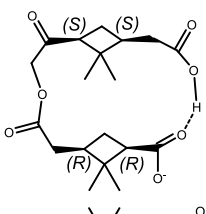
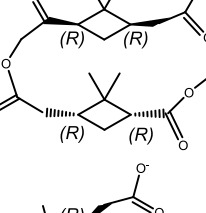
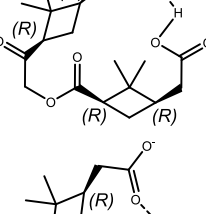
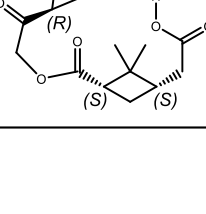
Abbreviation	Structure	$m/z$	$\Omega_{N_2}$ IMS ( $\text{\AA}^2$ )	$\Omega_{N_2}$ MOBCAL ( $\text{\AA}^2$ )	RD%	
357aHB(R)(S,S)		C <sub>17</sub> H <sub>25</sub> O <sub>8</sub> <sup>-</sup>	357.1549	178.6	188.2	5.27%

Table 4. Cont.

Abbreviation	Structure	<i>m/z</i>	$\Omega_{N_2}$ IMS ( $\text{\AA}^2$ )	$\Omega_{N_2}$ MOBCAL ( $\text{\AA}^2$ )	RD%	
357aHB(R)(R,R)		"	"	"	205.0	13.76%
357bHB(R)(R,R)		"	"	"	182.8	2.35%
357bHB(S)(S,S)		"	"	"	198.4	10.50%
367aHB(S,S)(R,R)		$C_{19}H_{27}O_7^-$	367.1757	182.5	192.2	5.19%
367aHB(R,R)(R,R)		"	"	"	193.0	5.56%
367bHB(R,R)(R,R)		"	"	"	185.1	1.42%
367bHB(R,R)(S,S)		"	"	"	195.7	6.97%

#### 4. Conclusions

Using UPLC/ESI(-)-IMS-QTOFMS, we obtained collision cross-section ( $\Omega_{N_2}$ ) values for the MS<sup>2</sup> product ions of two major dimeric compounds, namely  $m/z$  357 (C<sub>17</sub>H<sub>25</sub>O<sub>8</sub><sup>-</sup>) and  $m/z$  367 (C<sub>19</sub>H<sub>27</sub>O<sub>7</sub><sup>-</sup>), present in  $\alpha$ -pinene SOA. In addition to N<sub>2</sub>-IMS-TOFMS, the product ions were subjected to CO<sub>2</sub>-IMS-TOFMS for further structural characterisation. Obtained  $\Omega_{N_2}$  values and CO<sub>2</sub> drift times of product ions were compared to those of monomeric  $\alpha$ -pinene SOA standard compounds. Based on the results from a set of IMS-QTOFMS measurements, we conclude that the  $m/z$  357 (C<sub>17</sub>H<sub>25</sub>O<sub>8</sub><sup>-</sup>) ion consists of a terpenylic acid moiety and *cis*-pinic acid, and the  $m/z$  367 (C<sub>19</sub>H<sub>27</sub>O<sub>7</sub><sup>-</sup>) ion consists of 10-hydroxy-*cis*-pinonic acid and *cis*-pinic acid. To confirm their structures, possible structural isomers were evaluated through the comparison of measured and theoretical  $\Omega_{N_2}$  values. The results indicate that both  $m/z$  357 (C<sub>17</sub>H<sub>25</sub>O<sub>8</sub><sup>-</sup>) and  $m/z$  367 (C<sub>19</sub>H<sub>27</sub>O<sub>7</sub><sup>-</sup>) ions likely have an intra-molecular hydrogen bond between terminal carboxyl groups forming a clam shell structure in the IMS instrument. The measured and theoretical  $\Omega_{N_2}$  values of the  $m/z$  367 agreed very well with the structure that has all the chiral centres in an (*R*) configuration. This structure is consistent with the study of Kahnt et al. (2018) [19] that proposed an ester bond between the carboxylic group attached to the isobutyric part of pinic acid and the hydroxy group of the 2-hydroxy-3-methylbutanal part of 10-hydroxy-*cis*-pinonic acid. The structural elucidation for the  $m/z$  357 ion is not conclusive as RD% of measured and theoretical  $\Omega_{N_2}$  values was over 2%; the theoretical  $\Omega_{N_2}$  value was closer to the structure suggested by Gao et al. (2010) [22] and Beck and Hoffmann (2016) [20] than Yasmeeen et al. (2010) [21] and Kahnt et al. (2018) [19]. Further study is needed for a conclusive structural elucidation of the  $m/z$  357 ion.

**Author Contributions:** Conceptualisation, Y.I.; methodology, Y.I.; chemical synthesis, A.K. and R.S.; chamber experiment, S.R. and K.S.; ion mobility modelling and measurements, Y.I.; LC-MS experiments, Y.I.; writing—original draft preparation, Y.I.; writing—review and editing, Y.I., S.R., K.S., A.K., R.S.; funding acquisition, K.S. and S.R. All authors have read and agree to the published version of the manuscript.

**Funding:** K.S. and S.R. gratefully acknowledge financial support from JSPS KAKENHI JP17H01866.

**Institutional Review Board Statement:** Not applicable.

**Informed Consent Statement:** Not applicable.

**Data Availability Statement:** The raw data presented in this study are available on request from the corresponding author.

**Conflicts of Interest:** The authors declare no conflict of interest.

#### References

1. Hallquist, M.; Wenger, J.C.; Baltensperger, U.; Rudich, Y.; Simpson, D.; Claeys, M.; Dommen, J.; Donahue, N.M.; George, C.; Goldstein, A.H.; et al. The formation, properties and impact of secondary organic aerosol: Current and emerging issues. *Atmos. Chem. Phys.* **2009**, *9*, 5155–5236. [[CrossRef](#)]
2. Kim, K.-H.; Kabir, E.; Kabir, S. A review on the human health impact of airborne particulate matter. *Environ. Int.* **2015**, *74*, 136–143. [[CrossRef](#)] [[PubMed](#)]
3. Davidson, C.I.; Phalen, R.F.; Solomon, P.A. Airborne Particulate Matter and Human Health: A Review. *Aerosol. Sci. Technol.* **2005**, *39*, 737–749. [[CrossRef](#)]
4. Goldstein, A.H.; Galbally, I.E. Known and Unexplored Organic Constituents in the Earth's Atmosphere. *Environ. Sci. Technol.* **2007**, *41*, 1514–1521. [[CrossRef](#)] [[PubMed](#)]
5. Guenther, A.B.; Jiang, X.; Heald, C.L.; Sakyuanontvittaya, T.; Duhl, T.; Emmons, L.K.; Wang, X. The Model of Emissions of Gases and Aerosols from Nature version 2.1 (MEGAN2.1): An extended and updated framework for modeling biogenic emissions. *Geosci. Model Dev.* **2012**, *5*, 1471–1492. [[CrossRef](#)]
6. Nozière, B.; Kalberer, M.; Claeys, M.; Allan, J.; D'Anna, B.; Decesari, S.; Finessi, E.; Glasius, M.; Grgić, I.; Hamilton, J.F.; et al. The Molecular Identification of Organic Compounds in the Atmosphere: State of the Art and Challenges. *Chem. Rev.* **2015**, *115*, 3919–3983. [[CrossRef](#)]
7. Spolnik, G.; Wach, P.; Rudzinski, K.J.; Skotak, K.; Danikiewicz, W.; Szmigielski, R. Improved UHPLC-MS/MS Methods for Analysis of Isoprene-Derived Organosulfates. *Anal. Chem.* **2018**, *90*, 3416–3423. [[CrossRef](#)]



8. De Vijlder, T.; Valkenburg, D.; Lemièrre, F.; Romijn, E.P.; Laukens, K.; Cuyckens, F. A tutorial in small molecule identification via electrospray ionization-mass spectrometry: The practical art of structural elucidation. *Mass Spec. Rev.* **2018**, *37*, 607–629. [[CrossRef](#)]
9. Laphorn, C.; Pullen, F.; Chowdhry, B.Z. Ion mobility spectrometry-mass spectrometry (IMS-MS) of small molecules: Separating and assigning structures to ions. *Mass Spectrom. Rev.* **2013**, *32*, 43–71. [[CrossRef](#)]
10. Iinuma, Y.; Böge, O.; Kahnt, A.; Herrmann, H. Laboratory chamber studies on the formation of organosulfates from reactive uptake of monoterpene oxides. *Phys. Chem. Chem. Phys.* **2009**, *11*, 7985–7997. [[CrossRef](#)]
11. Krechmer, J.E.; Groessl, M.; Zhang, X.; Junninen, H.; Massoli, P.; Lambe, A.T.; Kimmel, J.R.; Cubison, M.J.; Graf, S.; Lin, Y.-H.; et al. Ion mobility spectrometry–mass spectrometry (IMS–MS) for on- and offline analysis of atmospheric gas and aerosol species. *Atmos. Meas. Tech.* **2016**, *9*, 3245–3262. [[CrossRef](#)]
12. Zhang, X.; Zhang, H.; Xu, W.; Wu, X.; Tyndall, G.S.; Orlando, J.J.; Jayne, J.T.; Worsnop, D.R.; Canagaratna, M.R. Molecular characterization of alkyl nitrates in atmospheric aerosols by ion mobility mass spectrometry. *Atmos. Meas. Tech.* **2019**, *12*, 5535–5545. [[CrossRef](#)]
13. Zhang, X.; Krechmer, J.E.; Groessl, M.; Xu, W.; Graf, S.; Cubison, M.; Jayne, J.T.; Jimenez, J.L.; Worsnop, D.R.; Canagaratna, M.R. A novel framework for molecular characterization of atmospherically relevant organic compounds based on collision cross section and mass-to-charge ratio. *Atmos. Chem. Phys.* **2016**, *16*, 12945–12959. [[CrossRef](#)]
14. Renard, P.; Tlili, S.; Ravier, S.; Quivet, E.; Monod, A. Aqueous phase oligomerization of  $\alpha,\beta$ -unsaturated carbonyls and acids investigated using ion mobility spectrometry coupled to mass spectrometry (IMS-MS). *Atmos. Environ.* **2016**, *130*, 153–162. [[CrossRef](#)]
15. Zhang, X.; Lambe, A.T.; Upshur, M.A.; Brooks, W.A.; Gray Bé, A.; Thomson, R.J.; Geiger, F.M.; Surratt, J.D.; Zhang, Z.; Gold, A.; et al. Highly Oxygenated Multifunctional Compounds in  $\alpha$ -Pinene Secondary Organic Aerosol. *Environ. Sci. Technol.* **2017**, *51*, 5932–5940. [[CrossRef](#)]
16. Zhao, Z.; Le, C.; Xu, Q.; Peng, W.; Jiang, H.; Lin, Y.-H.; Iii, D.R.C.; Zhang, H. Compositional Evolution of Secondary Organic Aerosol as Temperature and Relative Humidity Cycle in Atmospherically Relevant Ranges. *ACS Earth Space Chem.* **2019**, *3*, 2549–2558. [[CrossRef](#)]
17. Zhao, Z.; Tolentino, R.; Lee, J.; Vuong, A.; Yang, X.; Zhang, H. Interfacial Dimerization by Organic Radical Reactions during Heterogeneous Oxidative Aging of Oxygenated Organic Aerosols. *J. Phys. Chem. A* **2019**, *123*, 10782–10792. [[CrossRef](#)]
18. Zhao, Z.; Mayorga, R.; Lee, J.; Yang, X.; Tolentino, R.; Zhang, W.; Vuong, A.; Zhang, H. Site-Specific Mechanisms in OH-Initiated Organic Aerosol Heterogeneous Oxidation Revealed by Isomer-Resolved Molecular Characterization. *ACS Earth Space Chem.* **2020**, *4*, 783–794. [[CrossRef](#)]
19. Kahnt, A.; Vermeylen, R.; Iinuma, Y.; Safi Shalamzari, M.; Maenhaut, W.; Claeys, M. High-molecular-weight esters in  $\alpha$ -pinene ozonolysis secondary organic aerosol: Structural characterization and mechanistic proposal for their formation from highly oxygenated molecules. *Atmos. Chem. Phys.* **2018**, *18*, 8453–8467. [[CrossRef](#)]
20. Beck, M.; Hoffmann, T. A detailed MS<sub>n</sub> study for the molecular identification of a dimer formed from oxidation of pinene. *Atmos. Environ.* **2016**, *130*, 120–126. [[CrossRef](#)]
21. Yasmeen, F.; Vermeylen, R.; Szmigielski, R.; Iinuma, Y.; Böge, O.; Herrmann, H.; Maenhaut, W.; Claeys, M. Terpenylic acid and related compounds: Precursors for dimers in secondary organic aerosol from the ozonolysis of  $\alpha$  and  $\beta$ -pinene. *Atmos. Chem. Phys.* **2010**, *10*, 9383–9392. [[CrossRef](#)]
22. Gao, Y.; Hall, W.A.; Johnston, M.V. Molecular Composition of Monoterpene Secondary Organic Aerosol at Low Mass Loading. *Environ. Sci. Technol.* **2010**, *44*, 7897–7902. [[CrossRef](#)] [[PubMed](#)]
23. Kristensen, K.; Enggrob, K.L.; King, S.M.; Worton, D.R.; Platt, S.M.; Mortensen, R.; Rosenoern, T.; Surratt, J.D.; Bilde, M.; Goldstein, A.H.; et al. Formation and occurrence of dimer esters of pinene oxidation products in atmospheric aerosols. *Atmos. Chem. Phys.* **2013**, *13*, 3763–3776. [[CrossRef](#)]
24. Kourtchev, I.; Fuller, S.J.; Giorio, C.; Healy, R.M.; Wilson, E.; O'Connor, I.; Wenger, J.C.; McLeod, M.; Aalto, J.; Ruuskanen, T.M.; et al. Molecular composition of biogenic secondary organic aerosols using ultrahigh-resolution mass spectrometry: Comparing laboratory and field studies. *Atmos. Chem. Phys.* **2014**, *14*, 2155–2167. [[CrossRef](#)]
25. Kourtchev, I.; Doussin, J.-F.; Giorio, C.; Mahon, B.; Wilson, E.M.; Maurin, N.; Pangui, E.; Venables, D.S.; Wenger, J.C.; Kalberer, M. Molecular composition of fresh and aged secondary organic aerosol from a mixture of biogenic volatile compounds: A high-resolution mass spectrometry study. *Atmos. Chem. Phys.* **2015**, *15*, 5683–5695. [[CrossRef](#)]
26. Kristensen, K.; Watne, Å.K.; Hammes, J.; Lutz, A.; Peta, T.; Hallquist, M.; Bilde, M.; Glasius, M. High-Molecular Weight Dimer Esters Are Major Products in Aerosols from  $\alpha$ -Pinene Ozonolysis and the Boreal Forest. *Environ. Sci. Technol. Lett.* **2016**, *3*, 280–285. [[CrossRef](#)]
27. Docherty, K.S.; Wu, W.; Lim, Y.B.; Ziemann, P.J. Contributions of Organic Peroxides to Secondary Aerosol Formed from Reactions of Monoterpenes with O<sub>3</sub>. *Environ. Sci. Technol.* **2005**, *39*, 4049–4059. [[CrossRef](#)]
28. Ziemann, P.J. Formation of Alkoxyhydroperoxy Aldehydes and Cyclic Peroxyhemiacetals from Reactions of Cyclic Alkenes with O<sub>3</sub> in the Presence of Alcohols. *J. Phys. Chem. A* **2003**, *107*, 2048–2060. [[CrossRef](#)]
29. Davidson, K.L.; Bush, M.F. Effects of Drift Gas Selection on the Ambient-Temperature, Ion Mobility Mass Spectrometry Analysis of Amino Acids. *Anal. Chem.* **2017**, *89*, 2017–2023. [[CrossRef](#)]

30. Asbury, G.R.; Hill, H.H. Using Different Drift Gases to Change Separation Factors ( $\alpha$ ) in Ion Mobility Spectrometry. *Anal. Chem.* **2000**, *72*, 580–584. [[CrossRef](#)]
31. Kurulugama, R.T.; Darland, E.; Kuhlmann, F.; Stafford, G.; Fjeldsted, J. Evaluation of drift gas selection in complex sample analyses using a high performance drift tube ion mobility-QTOF mass spectrometer. *Analyst* **2015**, *140*, 6834–6844. [[CrossRef](#)] [[PubMed](#)]
32. Matz, L.M.; Hill, H.H.; Beegle, L.W.; Kanik, I. Investigation of drift gas selectivity in high resolution ion mobility spectrometry with mass spectrometry detection. *J. Am. Soc. Mass. Spectrom.* **2002**, *13*, 300–307. [[CrossRef](#)]
33. Fasciotti, M.; Sanvido, G.B.; Santos, V.G.; Lalli, P.M.; McCullagh, M.; de Sá, G.F.; Daroda, R.J.; Peter, M.G.; Eberlin, M.N. Separation of isomeric disaccharides by traveling wave ion mobility mass spectrometry using CO<sub>2</sub> as drift gas: Increasing ion mobility Synapt resolution with CO<sub>2</sub>. *J. Mass Spectrom.* **2012**, *47*, 1643–1647. [[CrossRef](#)] [[PubMed](#)]
34. Sato, K.; Hatakeyama, S.; Imamura, T. Secondary Organic Aerosol Formation during the Photooxidation of Toluene: NO<sub>x</sub> Dependence of Chemical Composition. *J. Phys. Chem. A* **2007**, *111*, 9796–9808. [[CrossRef](#)] [[PubMed](#)]
35. Ramasamy, S.; Nakayama, T.; Imamura, T.; Morino, Y.; Kajii, Y.; Sato, K. Investigation of dark condition nitrate radical- and ozone-initiated aging of toluene secondary organic aerosol: Importance of nitrate radical reactions with phenolic products. *Atmos. Environ.* **2019**, *219*, 117049. [[CrossRef](#)]
36. Akimoto, H.; Hoshino, M.; Inoue, G.; Sakamaki, F.; Washida, N.; Okuda, M. Design and characterization of the evacuable and bakable photochemical smog chamber. *Environ. Sci. Technol.* **1979**, *13*, 471–475. [[CrossRef](#)]
37. Claeys, M.; Iinuma, Y.; Szmigielski, R.; Surratt, J.D.; Blockhuys, F.; Van Alsenoy, C.; Böge, O.; Sierau, B.; Gómez-González, Y.; Vermeylen, R.; et al. Terpenylic Acid and Related Compounds from the Oxidation of  $\alpha$ -Pinene: Implications for New Particle Formation and Growth above Forests. *Environ. Sci. Technol.* **2009**, *43*, 6976–6982. [[CrossRef](#)]
38. Kołodziejczyk, A.; Pyrcz, P.; Pobudkowska, A.; Błaziak, K.; Szmigielski, R. Physicochemical Properties of Pinic, Pinonic, Norpinic, and Norpinonic Acids as Relevant  $\alpha$ -Pinene Oxidation Products. *J. Phys. Chem. B* **2019**, *123*, 8261–8267. [[CrossRef](#)]
39. Paglia, G.; Williams, J.P.; Menikarachchi, L.; Thompson, J.W.; Tyldesley-Worster, R.; Halldórsson, S.; Rolfsson, O.; Moseley, A.; Grant, D.; Langridge, J.; et al. Ion Mobility Derived Collision Cross Sections to Support Metabolomics Applications. *Anal. Chem.* **2014**, *86*, 3985–3993. [[CrossRef](#)]
40. Paglia, G.; Astarita, G. Metabolomics and lipidomics using traveling-wave ion mobility mass spectrometry. *Nat. Protoc.* **2017**, *12*, 797–813. [[CrossRef](#)]
41. Campuzano, I.; Bush, M.F.; Robinson, C.V.; Beaumont, C.; Richardson, K.; Kim, H.; Kim, H.I. Structural Characterization of Drug-like Compounds by Ion Mobility Mass Spectrometry: Comparison of Theoretical and Experimentally Derived Nitrogen Collision Cross Sections. *Anal. Chem.* **2012**, *84*, 1026–1033. [[CrossRef](#)] [[PubMed](#)]
42. Mesleh, M.F.; Hunter, J.M.; Shvartsburg, A.A.; Schatz, G.C.; Jarrold, M.F. Structural Information from Ion Mobility Measurements: Effects of the Long-Range Potential. *J. Phys. Chem.* **1996**, *100*, 16082–16086. [[CrossRef](#)]
43. Müller, L.; Reinnig, M.-C.; Hayen, H.; Hoffmann, T. Characterization of oligomeric compounds in secondary organic aerosol using liquid chromatography coupled to electrospray ionization Fourier transform ion cyclotron resonance mass spectrometry. *Rapid Commun. Mass Spectrom.* **2009**, *23*, 971–979. [[CrossRef](#)] [[PubMed](#)]
44. Müller, L.; Reinnig, M.-C.; Warnke, J.; Hoffmann, T. Unambiguous identification of esters as oligomers in secondary organic aerosol formed from cyclohexene and cyclohexene/ $\alpha$ -pinene ozonolysis. *Atmos. Chem. Phys.* **2008**, *8*, 1423–1433. [[CrossRef](#)]
45. Alelyunas, Y.W.; Smith, K.; Cleland, G.; Mortishire-Smith, R.; Wrona, M.D. Building a Collision Cross Section Library of Pharmaceutical Drugs Using the Vion IMS QT of Platform. Verification of System Performance, Precision and Deviation of CCS Measurements. *Waters Appl. Note* **2017**, 720005903. Available online: <https://www.waters.com/webassets/cms/library/docs/720005903en.pdf> (accessed on 7 December 2020).